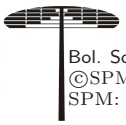
Bol. Soc. Paran. Mat. (3s.) **v. 00** 0 (0000): **??–??.**
©SPM –ISSN-2175-1188 ON LINE ISSN-00378712 IN PRESS
SPM: www.spm.uem.br/bspm doi:10.5269/bspm.41334

A New Partial Differential Equation for Image Inpainting *

M. Benseghir, F.Z. Nouri and P.C. Tauber

ABSTRACT: A considerable interest in the inpainting problem have attracted many researchers in applied mathematics community. In fact in the last decade, nonlinear high order partial differential equations have payed a central role in high quality inpainting developments. In this paper, we propose a technique for inpainting that combines an anisotropic diffusion process with an edge-corner enhancing shock filtering. This technique makes use of a partial differential equation that is based on a nonlinear structure tensor which increases the accuracy and robustness of the coupled diffusion and shock filtering. A methodology of partition and adjustment is used to estimate the contrast parameters that control the strength of the diffusivity functions. We focus on restoring large missing regions in grey scale images containing complex geometries parts. Our model is extended to a three dimensional case, where numerical experimentations were carried out on filling brain multiple sclerosis lesions in medical images. The efficiency and the competitiveness of the proposed algorithm is numerically compared to other approaches on both synthetic and real images.

Key Words: Partial Differential Equations, Image Inpainting, Shock Filtering.

Contents

1 Introduction **2**

2 Related works **3**
2.1 Linear structure tensor 3
2.2 Inpainting methods based on the LST 4

3 Proposed Model **5**
3.1 Nonlinear structure orientation 5
3.2 Proposed inpainting PDE 6
3.3 Extension to 3D 7
3.4 Contrast parameter approximation 8

4 Discretization and implementation **9**
4.1 Numerical stability 9
4.2 Implementation 11

5 Results and comments **12**

6 Conclusion **13**

* The project is supported by a Phd grant from MESRS
2010 *Mathematics Subject Classification:* Primary 35Q94, 68U10; Secondary 65M06, 65N12.
Submitted January 18, 2018. Published April 10, 2018

1. Introduction

Inpainting is the technique of reconstructing or restoring a damaged part of an image by using available information to filling-in the target region. It is widely used for digital image processing in different applications (e.g. recovering lost pixels, restoring old film, object and text removal, red-eye correction, super resolution reconstruction, etc.). Nowadays, there are three categories of inpainting approaches: methods based on the synthesis of textures [12], [13], [14], [16], [17], [24] and [32], geometric methods [3], [5], [9], [10], [19], [20], [27] and [28] and hybrid methods [4], [15] and [23] . The first are based on searching and copying similar patches in the neighborhood of the damaged region, where the reconstruction is done from the outside to the inside edge of the target area; for example, Criminisi et al. [12] adopt an order to fill in the missing region where the patches of the high gradient zones are processed first. These methods give very effective solutions for the reconstruction of textures but do not handle very effectively edges and boundaries. The second family artificially synthesizes an image compatible with the human visual system. The main idea of these approaches is to restore photometric and structural information such as edges, corners, curvatures and junctions. In these approaches, the target region is filled by diffusing the information from their surroundings using partial differential equations (PDEs). It is very common in such models to use functions to control the diffusion strength. These functions are however very sensitive to the choice of the so-called contrast threshold parameters that are specific to each image due to their sensitivity to the local change of brightness. Finally, the last category of approaches, namely "the hybrid methods", try to take the advantages of the first two classes of methods to ensure the reconstruction of both the geometric and the textured components.

In this paper, we propose an inpainting technique based on the non-linear structure tensor (NLST) estimations in order to evaluate more precisely the local anisotropy of the image data and the orientation of the diffusion. To preserve the image geometric properties, an oriented diffusion process is coupled with edge-and-corner shock filtering, for reconstructing (or restoring) large missing regions in grayscale images containing complex geometries. The contrast parameters of the different terms are estimated. A numerical scheme supported by a new algorithm is presented along with numerical results confirming the efficiency and competitiveness of the method in terms of Peak Signal to Noise Ratio (PSNR), Structural Similarity Measure (SSIM) and visual quality, compared to several other inpainting approaches [9], [26] and [33].

Furthermore, a 3D version of our model applied to volumetric data is presented. It is well known that in medical imaging, a presence of multiple sclerosis (MS) lesions in brain affect magnetic resonance imaging (MRI) processing, such as registration, brain volume measurements, automated tissue classification tools etc... Multiple patch-based image inpainting techniques have been proposed to filling lesions that considerably reduce the impact of MS in many MRI analysis protocols (see for example [1], [11], [18] and [25]). Here, we are interested to analyse and experiment numerically the proposed PDE-based model for this application.

This paper is organized as follows: in section 2, we present some related works from the inpainting domain, outlining their advantages and limitations and highlighting our contribution. Section 3 is devoted to the presentation of the proposed model in 2D and extended to a three dimensional case. The numerical analysis and implementation are summarized in section 4, and the results and comments are detailed in section 5. We finish with concluding remarks.

2. Related works

Since the work of Perona-Malik [21], the anisotropic diffusion PDEs were largely developed for multiple applications in image processing. Their principle is based on the application of successive locally oriented diffusion of the image pixels intensity, which is controlled to preserve important structures. Diffusion based inpainting was the first digital inpainting approach [3]. This technique mainly uses nonlinear PDEs and variational approaches to propagate the information in direction of level lines, by minimizing an energy functional. For example, the popular total variation (TV) model, proposed by chan et al. [9], is based on the minimization of the TV norm with the efficiency to restore degraded and noised images for only small missing regions, however it fails to realize the connectivity principle in visual perception. Most of PDE-based inpainting techniques use the gradient vector to estimate edges orientation, unfortunately it can never provide a truly accurate estimation in features with complex geometries, as it does not allow us to distinguish between corners and straight edges. Recently, the most popular estimator is the structure tensor, also known as second moment matrix; that is frequently used in oriented diffusion filtering [22], [26], [28], [30] and [31], with the performance to give an accurate estimation of image structure orientations, particularly when edges are oriented uniformly.

2.1. Linear structure tensor

Feature extraction and orientation estimation are very important for image processing and computer vision communities. The most popular estimator is the linear structure tensor (LST), given by

$$L = G_\rho * \left(\nabla U \nabla U^T\right) = \begin{pmatrix} G_\rho * (U_x)^2 & G_\rho * (U_x U_y) \\ G_\rho * (U_x U_y) & G_\rho * (U_y)^2 \end{pmatrix} \tag{2.1}$$

where U is the image and ρ is a scale factor of the Gaussian kernel. The convolution $(\nabla U \nabla U^T)$ with the Gaussian kernel $G(0, \rho^2)$ does not only reduce the noise level, but also introduces a spatial coherence through the scale factor ρ and makes structure analysis insensitive to textures. Sometimes, U is also smoothed by another Gaussian kernel $G(0, \sigma^2)$, with σ the variance, to make the tensor even more robust to noise. The matrix L is symmetric and positive semi-definite with maximum and minimum eigenvalues λ^+ and λ^-, respectively, and the corresponding orthonormal eigenvectors V and $V^\perp$. The vector V represents the orientation with the highest gray value fluctuation $(V//\nabla U)$ and $V^\perp$ gives the best local orientation

$(V^{\perp}//\nabla U^{\perp})$, i.e. the *coherence direction*. The analysis of eigenvalues and eigenvectors of L provides useful information about the complexity of local structures in a neighborhood of each pixel in U, for more details see [2].

2.2. Inpainting methods based on the LST

By taking into account the advantages of the LST, new methods of inpainting have been developed. For instance, in order to better protect the edge and corner structures during the restoration process, Zhang and al. [33] have proposed the following anisotropic PDE that exploits the amplitude information contained in the LST:

$$\frac{\partial U}{\partial t} = f(c).f(|\nabla U|)U_{\eta\eta} + \alpha U_{\xi\xi}, \tag{2.2}$$

where $U_{\eta\eta} = D^2U(\eta,\eta)$ and $U_{\xi\xi} = D^2U(\xi,\xi)$ are second-order directional derivatives in the gradient $(\eta = \frac{\nabla U}{||\nabla U||})$ and tangential direction $(\xi = \frac{\nabla^{\perp} U}{||\nabla U||})$ respectively, and $\alpha > 0$ is set to be a large diffusion coefficient. The functions that control the diffusion strength along the gradient direction are, the corner protection function $f(c) = \frac{1}{1+\left(\frac{c}{K}\right)^2}$, and the edge stopping function $f(|\nabla U|) = \frac{1}{1+\left(\frac{|\nabla U|}{K}\right)^2}$, where $c = |(\nabla \cdot (V^{\perp}V^{\perp T}))^T \cdot \nabla U|$ is the corner intensity at each pixel and K an adaptive contrast parameter. Note that (η, ξ) are the characteristics parameters.

It has to be pointed out that equation (2.2) can preserve corner and edge features during an inpainting procedure, however it does not restore corners in large missing regions. In addition, this approach does not consider the orientation information contained in the LST.

To overcome some of these limitations, Shao et al. [26] proposed the following PDE:

$$\begin{aligned}\frac{\partial U}{\partial t} = {} & f_V.U_{VV} + f_{V^{\perp}}.U_{V^{\perp}V^{\perp}} - \gamma.sign(U_{VV}).||\nabla U_{\sigma}|| \\ & -(f_{V^{\perp}} - f_V)((\nabla \cdot (V^{\perp}V^{\perp T}))^T \cdot \nabla U_{\sigma})\end{aligned} \tag{2.3}$$

The robust orientation diffusion PDE (2.3) is the generalization of the directional diffusion of Perona-Malik, used for many applications, such as denoising, inpainting, super-resolution reconstruction, etc.. The eigenvectors of (2.3), V and $V^{\perp}$ are the robust orientations derived from LST, substituted for the gradient and tangential directions, respectively. The functions f_V and $f_{V^{\perp}}$ are the edge stopping functions, chosen as $f_V = f_V(|\lambda^+ - \lambda^-|) = \frac{1}{1+|\lambda^+ - \lambda^-|}$ and $f_V = f_{V^{\perp}}(|\lambda^+ - \lambda^-|) = \frac{1}{1+|\lambda^+ - \lambda^-|^a}$, where λ^+ and λ^- are the maximum and minimum eigenvalues of (2.1) and $0 < a \leq 1$. Note that Tschumperlé [28] presented a similar PDE, with only the first two terms in (2.3) that is not able to preserve corner structures. The third term in (2.3) is an edge shock filter, where γ is a small positive control parameter. This term is added to favor both the smoothness and the sharpness of edge structures. The last term is a corner shock filter.

While it was shown that this model can better preserve the corner structures, as well as allows to restrain the rounding artifacts, its performances fall when dealing with large areas covering sharp or curved edges. Furthermore, the Gaussian smoothing used in the LST induces dislocation of discontinuities and blurring effects.

3. Proposed Model

To overcome the disadvantages of the previous models, we propose an inpainting technique based on a NLST, a more adaptive structure estimator that gives a better estimation of image structure orientations than their linear counterpart LST. In the proposed approach, an edge and corner shock filters based on the NLST are used to enhance and protect structures during filling-in process. The strength of diffusion is controlled through several stopping functions carefully selected to ensure a good compromise between the robust orientation diffusion and the shock filtering. Furthermore, to avoid the inconvenient choice of several constants in an adaptive manner, a partition and an adjustment methodologies are proposed to estimate the contrast parameters that control the force of the diffusivity functions.

3.1. Nonlinear structure orientation

In this subsection we present the principle of NLST, as initially proposed by Weickert et al. [8], and study the advantages of the NLST compared to the LST model (2.1). We recall that the estimation of the linear structure tensor in (2.1) can be modeled by the diffusion equation

$$\begin{cases} \frac{\partial s_{p,q}}{\partial t} = \Delta s_{p,q}, \\ S_0 = \nabla U \nabla U^T = (s^0_{p,q}), i, j = 1, 2, \end{cases} \tag{3.1}$$

where the diffusion time t is related to the standard deviation ρ of the Gaussian in (2.1) via $t = \frac{\rho^2}{2}$. The NLST replaces the diffusion equation (3.1) by an anisotropic diffusion to reduce smoothing in the presence of edges and enhance the image structure. This process is given by

$$\frac{\partial s_{p,q}}{\partial t} = div[g(|\lambda_{\max} - \lambda_{\min}|)\nabla s_{p,q}], \quad p, q = 1, 2, \tag{3.2}$$

where $g(r) = \frac{1}{\sqrt{\varepsilon^2 + (\frac{r}{k})^2}}$ is the diffusivity function, with $\varepsilon > 0$ a small fixed parameter used to avoid singularities, $k > 0$ and the measure $r = |\lambda_{\max} - \lambda_{\min}|$ determines the coherence in the image data ($\lambda_{\max}, \lambda_{\min}$ are the maximum and minimum eigenvalues of S). When applying a diffusion process to the matrix-valued data $S = (s_{ij})_{i,j=1,2}$, the positive semi-definiteness of the original data S_0 is preserved and the maximum-minimum principle for the field of the eigenvalues associated with a matrix field is guaranteed (for more details the reader is referred to [8]). By using the eigenvalue decomposition, the NLST S can be expressed as follows:

$$S = \begin{pmatrix} V_1 & V_2 \end{pmatrix} \begin{pmatrix} \lambda_{\max} & 0 \\ 0 & \lambda_{\min} \end{pmatrix} \begin{pmatrix} V_1^T \\ V_2^T \end{pmatrix} \tag{3.3}$$

The eigenvector V_1, corresponding to $\lambda_{\max}$, represents the direction of the maximum signal variation while the eigenvector V_2, associated to $\lambda_{\min}$, gives the structure orientation. By analyzing the eigenvalues of the NLST, the measure $r = |\lambda_{\max} - \lambda_{\min}|$ gives very good information about the local image anisotropy so that in the homogeneous regions $|\lambda_{\max} - \lambda_{\min}| \approx 0$, in neighbourhood of straight

edges $|\lambda_{\max} - \lambda_{\min}| \gg 0$, but in the presence of junctions, corners or a curves $|\lambda_{\max} - \lambda_{\min}| > 0$. Compared with the conventional structure tensor (2.1), the NLST (3.3) has been highlighted as being able to more accurately estimate the structure orientation. It has several advantages, such as directional smoothing, edge enhancing and it avoids the dislocation of discontinuities. Considering these advantages, we make use of the NLST to build a novel inpainting approach that is suitable for images with both simple and complex geometries.

3.2. Proposed inpainting PDE

In this paper, we propose a coupled oriented diffusion and shock filtering PDE to fill in missing or damaged region. It is based on the estimations provided by (3.3) to determine the strength and direction of the diffusion. For simplicity, we first consider an analysis in two dimensional. This process is set as follows: we write

$$\begin{array}{c} \frac{\partial U}{\partial t} = f_1.U_{V_1V_1} + f_2.U_{V_2V_2} \\ -f_3.sign(U_{V_1V_1}).||\nabla U|| - f_4.((\nabla \cdot (V_2V_2^T))^T \cdot \nabla U) \end{array} \tag{3.4}$$

where $U_{V_1V_1} = D^2U(V_1, V_1)$ and $U_{V_2V_2} = D^2U(V_2, V_2)$ are the second derivatives in the directions V_1 and V_2 and the stopping functions are given by

$$f_1(r, k_1) = \begin{cases} \frac{1}{2}[1 - (\frac{r}{k_1\sqrt{2}})^2] & \text{if } r \leq k_1\sqrt{2} \\ 0 & \text{else} \end{cases} \tag{3.5}$$

and

$$f_2(r, k_2) = \frac{1}{(1 + \frac{r}{k_2})^a}, \text{ with } r = |\lambda_{\max} - \lambda_{\min}| \tag{3.6}$$

where a is a constant that was empirically set to 0.3 and $(k_i)_{i=1,2}$ are parameters that are semi-automatically estimated, as described hereafter. Note that f_1 gives a weak diffusion in the orthogonal direction to the contour, as long as the variation of the image intensity is small enough to avoid the effect of scaling and thus gives a natural effect to a restoration result (see for example **[6]**). The function f_2 used in **[26]**, encourages strong diffusion along the contours. This guarantees the reconstruction of geometric structures and ensures the continuity of the level lines. The last two terms in (3.1) are the shock filters for contours and angles, given by

$$f_3(r, k_3) = e^{\frac{-|\lambda_{\max} - \lambda_{\min}|^2}{k_3^2}} \tag{3.7}$$

and

$$f_4(C, k_4) = e^{-\frac{C}{k_4^2}} \tag{3.8}$$

where $C = |\nabla \cdot (V_2V_2^T))^T \cdot \nabla U|$ is the intensity of the angle, the parameters k_3 and k_4 will be specified later. The functions f_1, f_2, f_3 and f_4 are monotonically decreasing in $[0, 1]$, such that f_3 and $f_4$decrease faster than f_1 and f_2. Thus, this

adopted shock filtering decreases the diffusion in presence of significant discontinuities, with the possibility of preserving and enhancing the image structures in the following way:

(a) In homogeneous regions, only the first two terms in (3.4) are significant and we obtain an isotropic diffusion.

(b) In the neighborhood of a straight contour, the diffusion becomes anisotropic (strong in the most coherent direction) and the shock filter in the third term of (3.4) preserves the contours.

(c) In the presence of a corner, the diffusion is strong along the structures and the shock filter of the last two terms in (3.4) enhances the structure.

3.3. Extension to 3D

To validate these results, it would be more interesting if we extend our study to a three dimensional case by writing (3.4) as

$$\begin{array}{c} \frac{\partial U}{\partial t} = f_{V_1}.U_{V_1V_1} + f_{V_2}.U_{V_2V_2} + f_{V_3}.U_{V_3V_3} \\ -f_E.sign(U_{V_1V_1}).||\nabla U|| - f_c.((\nabla \cdot (V_3V_3^T))^T \cdot \nabla U) \end{array} \tag{3.9}$$

Note that we have three eigenvectors V_1, V_2 and V_3 associated to the eigenvalues λ_1, λ_2 and λ_3 such that $\lambda_1 \geq \lambda_2 \geq \lambda_3$, leading to an extra term $f_{V_3}U_{V_3V_3}$. Here the edges will be surfaces, so by taking into account the highest grey value fluctuations given by V_1, we choose

$$f_{V_1} = f_1(|\lambda_1 - \lambda_3|, k_1) \tag{3.10}$$

in order to stop diffusion across the surface structures ($|\lambda_1 - \lambda_3| \gg 0$). Hence we can point out that as long as the iso-surfaces are homogeneous ($|\lambda_2 - \lambda_3| \approx 0,$) the diffusion will be isotropic in the tangent plane. However when the surface is not isotropic, diffusion should be performed primarily along the best local orientation V_3. These goals are fulfilled by taking

$$f_{V_2} = f_2(|\lambda_1 - \lambda_2|, k_2), \tag{3.11}$$

$$f_{V_3} = f_2(|\lambda_2 - \lambda_3|, k_3) \tag{3.12}$$

Finally, the shock filters in the two last terms in (3.9), are controlled by

$$f_E = f_3(|\lambda_1 - \lambda_3|, k_4) \tag{3.13}$$

and

$$f_C = f_4(|\nabla \cdot (V_3V_3^T))^T \cdot \nabla U|, k_5), \tag{3.14}$$

prevent blurring effect near the geometric structures, where $(f_i)_{i=1}^4$ are given by (3.5), (3.6), (3.7) and (3.8), respectively and $(k_i)_{i=1}^5$ are the contrast parameters.

3.4. Contrast parameter approximation

Inspired by the work of Borroto-Fernández et al. [7], here we use a methodology of partition based on K-means algorithm and a least-square fit (KMLS) to approximate the contrast parameters in accordance with the local anisotropy measure and the corner intensity given by the NLST.

The diffusion coefficients $f(r,k)$ are monotonically decreasing functions $\in [0,1]$, and are very sensitive to the choice of the contrast parameters such that in the neighborhood of edges $(r > k)$ the smoothing effect is lower and the structures are preserved, but near homogeneous regions $(r < k)$ the smoothing effect is stronger. This means that these parameters interfere in one way or another with the diffusion process and are chosen according to the variation of the image photometric data, which differs from one image to another.

In order to approximate the contrast parameters at each iteration, we give a technique for a good constant selection. This process is based on a partitioning and adjustment methodologies which are carried out in the following two steps:

Step 1 : Partition
Let $f(r,k)$ be a diffusion function

- The set of pixels of the image P is partitioned into three clusters: P_1 for the pixels (x,y) in the homogeneous regions, P_3 for those in the neighborhood of edges and $P_2 = P \backslash (P_1 \cup P_3)$.

(a) Selection of initial means:

$$\begin{array}{ll} m_1 = \min\{r(x,y),(x,y) \in P\} & for\ P_1, \\ m_3 = \max\{r(x,y),(x,y) \in P\} & for\ P_3, \\ m_2 = \frac{m_1+m_3}{2} & for\ P_2. \end{array} \tag{3.15}$$

(b) Pixels affectation:

$$(x,y) \in P_i\ if\ d(r(x,y),m_i)_{i=1}^{3} = \min|r(x,y) - m_i|. \tag{3.16}$$

(c) Compute the new means to be the centroids of clusters.

$$m_i = \sum_{(x,y)\in P_i} \frac{r(x,y)}{n_i},\ i = 1,2,3 \tag{3.17}$$

where n_i is the number of pixels of each cluster P_i $(i = 1,2,3)$.
Operations (b) and (c) are repeated up to an equilibrium state.

(d) Selection of final means:

$$\begin{array}{l} m_1 = \max\{r(x,y),(x,y) \in P_1\} \\ m_3 = \min\{r(x,y),(x,y) \in P_3\} \end{array} \tag{3.18}$$

Step 2 : adjustment

The least squares fit method is applied to the diffusion functions f with the values m_1, m_3 given by (3.18) and the values *sep* a strong edge preserving threshold and *wep* a weak edge preserving threshold. This is equivalent to estimate the parameters k_i by minimizing, the following function:

$$S(k_i) = [sep - f_i(m_1, k_i)]^2 + [wep - f_i(m_3, k_i)]^2 \tag{3.19}$$

using the gradient descent method.
Note that, for the 3D case, we consider $r(x, y, z)$ and voxels instead of pixels.

4. Discretization and implementation

To solve equation (3.4) in accordance with the new contrast parameters $k_i(t)$,$i = 1, 2, 3$ and 4, we propose a finite difference numerical method based on a time-forward and space-centred scheme, satisfying an appropriate numerical stability condition (CFL condition). We write

$$\begin{array}{c} U_{i,j}^{n+1} = U_{i,j}^n + \tau[f_1^n.U_{V_1^n V_1^n}^n + f_2^n.U_{V_2^n V_2^n}^n \\ -f_3^n \cdot sign(U_{V_1^n V_1^n}^n).||\nabla U^n|| \\ -f_4^n((\nabla \cdot (V_2^n V_2^{nT}))^T \cdot \nabla U^n)]_{i,j} \end{array} \tag{4.1}$$

with $U_{i,j}^n = U(t_n, x_i, y_j)$ and $\tau = \Delta t$ the time step.
In the 3D case $U_{i,j,l}^n = U(t_n, x_i, y_j, z_l)$ and (4.1) becomes

$$\begin{array}{c} U_{i,j,l}^{n+1} = U_{i,j,l}^n + \tau[f_{V_1}^n.U_{V_1^n V_1^n}^n + f_{V_2}^n.U_{V_2^n V_2^n}^n + f_{V_3}^n.U_{V_3^n V_3^n}^n \\ -f_E^n \cdot sign(U_{V_1^n V_1^n}^n).||\nabla U^n|| \\ -f_C^n((\nabla \cdot (V_3^n V_3^{nT}))^T \cdot \nabla U^n)]_{i,j,l} \end{array} \tag{4.2}$$

First, we derive a stability condition to ensure the convergence properties of the proposed scheme, then we outline the associated resolution algorithm.

4.1. Numerical stability

In this subsection, we derive the stability conditions for our numerical scheme.

Proposition 4.1. *The numerical scheme (4.1) satisfy the following stability condition* $\tau = \Delta t \leq \frac{1}{2\ (f_1 + f_2 + P)}$ *with* $P = \frac{v_1.v_2.(f_1 - f_2)}{2(v_1^2 + v_2^2)}$, *according to a choice of space steps* $h = 1$.

Proof: To prove this result we proceed by Fourier analysis. Let us consider

$$\frac{\partial U}{\partial t} = f_1.D^2U(V_1, V_1) + f_2.D^2U(V_2, V_2) \tag{4.3}$$

where $V_1 = V_2^{\perp} = \begin{pmatrix} v_1 \\ v_2 \end{pmatrix}$ are eigenvectors of the NLS. Thus, we can write:

$$\frac{\partial U}{\partial t} = f_1.\frac{v_1^2 U_{xx} + 2v_1 v_2 U_{xy} + v_2^2 U_{yy}}{v_1^2 + v_2^2} + f_2.\frac{v_2^2 U_{xx} - 2v_1 v_2 U_{xy} + v_1^2 U_{yy}}{v_1^2 + v_2^2}$$

$$= \frac{(f_1 v_1^2 + f_2 v_2^2).U_{xx} + (f_1 v_2^2 + f_2 v_1^2).U_{yy} + 2v_1 v_2 (f_1 - f_2).U_{xy}}{v_1^2 + v_2^2}. \tag{4.4}$$

If we choose $\Delta x = \Delta y = 1$, the discrete scheme of (4.4) is written as

$$\begin{aligned} U_{i,j}^{n+1} &= U_{i,j}^n + \Delta t\big[A_1.(U_{i+1,j}^n - 2U_{i,j}^n + U_{i-1,j}^n) \\ &\quad + A_2.(U_{i,j+1}^n - 2U_{i,j}^n + U_{i,j-1}^n. \\ &\quad + A_3.(U_{i+1,j+1}^n + U_{i-1,j-1}^n - U_{i+1,j-1}^n - U_{i-1,j+1}^n)\big], \end{aligned} \tag{4.5}$$

where

$$A_1 = \frac{f_1 v_1^2 + f_2 v_2^2}{v_1^2 + v_2^2},$$

$$A_2 = \frac{f_1 v_2^2 + f_2 v_1^2}{v_1^2 + v_2^2}$$

and

$$A_3 = \frac{1}{4}\frac{2v_1 v_2 (f_1 - f_2)}{v_1^2 + v_2^2}.$$

By Fourier analysis, we substitute a solution of the form $U_{i,j}^n = \hat{U}^n e^{I\pi h(ki+mj)}$ with k and m are fixed modes and $I^2 = -1$, in quation (4.5) to get

$$\begin{aligned} \hat{U}^{n+1} e^{I\pi h(ki+mj)} &= \hat{U}^n e^{I\pi h(ki+mj)} \\ &\quad + \Delta t.\Big[A_1.(\hat{U}^n e^{I\pi h(k(i+1)+mj)} \\ &\quad - 2\hat{U}^n e^{I\pi h(ki+mj)} + \hat{U}^n e^{I\pi h(k(i-1)+mj)}) \\ &\quad + A_2.(\hat{U}^n e^{I\pi h(ki+m(j+1))} \\ &\quad - 2\hat{U}^n e^{I\pi h(ki+mj)} + \hat{U}^n e^{I\pi h(ki+m(j-1))}) \\ &\quad + A_3.(\hat{U}^n e^{I\pi h(k(i+1)+m(j+1))} + \hat{U}^n e^{I\pi h(k(i-1)+m(j-1))} \\ &\quad - \hat{U}^n e^{I\pi h(k(i+1)+m(j-1))} - \hat{U}^n e^{I\pi h(k(i-1)+m(j+1))})\Big]. \end{aligned} \tag{4.6}$$

By dividing by $e^{I\pi h(ki+mj)}$, and put $k\pi h = a_k$ and $m\pi h = b_m$,we get

$$\begin{aligned} \hat{U}^{n+1} = \hat{U}^n[1 + \Delta t(A_1.(2\cos(a_k) - 2) + A_2.(2\cos(b_k) - 2) \\ + A_3.(2\cos(a_k + b_k) - 2\cos(a_k - b_k)], \end{aligned} \tag{4.7}$$

leading to

$$\hat{U}^{n+1} = \hat{U}^n\big[1 + \Delta t\ [A_1.(-4\sin^2(\frac{a_k}{2})) + A_2.(-4\sin^2(\frac{b_k}{2})) \tag{4.8}$$

$$+ A_3.(-4\sin(a_k)\sin(b_k))]\big]. \tag{4.9}$$

The scheme is stable if $|\frac{\hat{U}^{n+1}}{\hat{U}^n}| \leq 1$. Thus we obtain

$$\left|1 - 4\Delta t\left[A_1.(\sin^2(\frac{a_k}{2})) + A_2.(\sin^2(\frac{b_k}{2})) + A_3.(\sin(a_k)\sin(b_k))\right]\right| \leq 1 \tag{4.10}$$

This implies that

$$\left|\frac{\hat{U}^{n+1}}{\hat{U}^n}\right| \leq |1 - 4\Delta t\,[A_1 + A_2 + A_3]| \leq 1 \quad \Longrightarrow 0 \leq \Delta t \leq \frac{1}{2[A_1 + A_2 + A_3]} \quad (4.11)$$

where $A_1 + A_2 + A_3 = \frac{f_1 v_1^2 + f_2 v_2^2}{v_1^2+v_2^2} + \frac{f_1 v_2^2 + f_2 v_1^2}{v_1^2+v_2^2} + \frac{v_1 v_2 (f_1 - f_2)}{2(v_1^2+v_2^2)} = f_1 + f_2 + \frac{v_1 v_2 (f_1 - f_2)}{2(v_1^2+v_2^2)}$, i.e we get the required result.This yields to a choice for the temporal discretisation parameter satisfying $\triangle t \leq \frac{2}{9}$. In a similar way, we can derive a stability condition for the 3D case. □

4.2. Implementation

For numerical investigations, we propose the following algorithms:

Algorithm 4.2. *Estimation of the orientation and local structure measures*

1 - Initialisation : input time step Δt, the number of iterations T_1 and the contrast parameter k.

2 - Approximate the space partial derivatives $\frac{\partial U^n}{\partial x}$, $\frac{\partial U^n}{\partial y}$, $\frac{\partial^2 U^n}{\partial x^2}$, $\frac{\partial^2 U^n}{\partial y^2}$ and $\frac{\partial^2 U^n}{\partial x \partial y}$, using a central finite difference scheme.

3 - Compute the structure tensor S_0^n from (3.2).

4 - Compute the initial eigenvalues $\lambda^n_{\max}$, and $\lambda^n_{\min}$

5 - Compute the elements of the NLST by:

$$\frac{s^{n+1}_{p,q} - s^n_{p,q}}{\Delta t} = div[g(|\lambda^n_{\max} - \lambda^n_{\min}|)\nabla s^n_{p,q}]$$

6 - If the number of iterations is less than T_1, repeat step 5.

7 - Compute $\lambda^n_{\max}, \lambda^n_{\min}$; V_1 and V_2 from (3.3).

8 - Compute the local contrast $r^n = |\lambda^n_{\max} - \lambda^n_{\min}|$ and the corner intensity

$$C^n = |(\nabla \cdot (V_2^n {V_2^n}^T))^T \cdot \nabla U^n|.$$

Algorithm 4.3. *Computation of the contrast parameters*

Step 1: Partition

1- Initialisation: selection of initial means

2- Affectation of pixels from (3.10) and compute the new means by (3.11), this is repeated up to an equilibrium state,

3- Selection of final means via (3.12),

Step 2: adjustment *Compute the contrast parameters k_i from (3.13),*

Algorithm 4.4. *Computation of the inpainted image*

1- Initialisation :Input a masked image U^0, time step τ and the number of iterations T.

*3- Estimate the orientation and local structure measures by **Algorithm 2**.*

*4- Compute f_1^n, f_2^n, f_3^n and f_4^n using the contrast parameters k_1, k_2, k_3 and k_4 estimated by **Algorithm 3**.*

5- Compute $U^n_{V_1^n V_1^n}$ and $U^n_{V_2^n V_2^n}$ defined in (4.1).

6- Compute the shock filters :

$-sign(U^n_{V_1^n V_1^n})||\nabla U^n_\sigma|$, $-((\nabla.(V_2^n {V_2^n}^T))^T.\nabla U^n_\sigma)$.

7- Compute U^{n+1} *from (4.1).*

8- While the number of iterations is $< T$ *stop, else repeat steps 3 to 7.*

For the 3D case, we adapt the above algoritms as follows:
In **Algorithm 2**:
Step 2: approximate $\frac{\partial U^n}{\partial z}$, $\frac{\partial^2 U^n}{\partial z^2}$, $\frac{\partial^2 U^n}{\partial x \partial z}$ and $\frac{\partial^2 U^n}{\partial y \partial z}$.
Step 4: compute the initial eigenvalues λ_1^n, λ_2^n and λ_3^n.
Step 5: compute the elements of the NLST with $|\lambda_1^n - \lambda_3^n|$.
Step 7: compute $(\lambda_i^n)_{i=1}^3$ and the corresponding eigenvectors $(V_i^n)_{i=1}^3$.
Step 8: store the measures $|\lambda_1^n - \lambda_2^n|$, $|\lambda_1^n - \lambda_2^n|$, $|\lambda_1^n - \lambda_2^n|$ and $|\nabla \cdot (V_3^n {V_3^n}^T))^T \cdot \nabla U^n|$.
In **Algorithm 4**:
Step 4: compute $f^n_{V_1}$, $f^n_{V_2}$, $f^n_{V_3}$, f^n_E and f^n_C using the contrast parameters $(k_i^n)_{i=1}^5$ estimated by **Algorithm 3**.
Step 6: compute $U^n_{V_3^n V_3^n}$ and $-\nabla \cdot (V_2^n {V_2^n}^T))^T \cdot \nabla U^n$.
Step 7: Compute U^{n+1} from (4.2).

5. Results and comments

In this section, the results obtained are compared with the ones resulted from Zhang et al. [33] (ZH), Shao et al. [26] (SH) and Chan et al. [9] (TV) algorithms. These results are analyzed using different approaches visual quality, peak signal noise ratio (PSNR) and structural similarity measure (SSIM) [29].

All computations are carried out on synthetic and real images using Matlab (R2012a) on a personal computer with 4 Core 2.40GHz CPU and 4GO of RAM.

According to [26] and [33] since we did not experienced any significant sensitivity to experimental results, some parameters are chosen to be fixed constants: for (ZH) approach we take $\sigma = 1.5$, $\rho = 2$, $\alpha = 1$ and $k = 5.$, while for (SH) $\sigma = 1.5$, $\rho = 2$, $\gamma = 0.01$ and $a = 0.3$. The time step is chosen to be $\tau = 0.2$ for all methods.

For the NLST algorithm the parameters are set as: the time step $\tau = 0.1$, $k = 4$ and a number of iteration $T_1 = 10$ is sufficient to get a satisfactory result. The strong and weak edge preserving thresholds are chosen to be $sep = 0.01$ and $wep = 0.5$. The principle of determining the number of iterations T is based on our perceptual quality of the inpainted images and the values of PSNR and SSIM.

The obtained numerical results are summarized as follows:

Models	Measures	Figure 1	Figure 2	Figure 3	Figure 4
TV	PSNR	24.55	20.05	30.11	25.51
	SSIM	0.7757	0.8302	0.9489	0.9311
ZH	PSNR	32.17	24.08	28.82	25.24
	SSIM	0.7858	0.8711	0.9466	0.9305
SH	PSNR	30.66	24.17	30.62	25.49
	SSIM	0.8220	0.8862	**0.9538**	0.9281
Our model	PSNR	**35.65**	**26.99**	**31.01**	**27.18**
	SSIM	**0.8636**	**0.9155**	0.9475	**0.9455**

Table 1: PSNR and SSIM values of inpainted images using the different approaches.

In **Figure 1-4**, we notice that the visual results are more or less close, but in our approach, the image is closer to the original one, with less blur and a more apparent geometric features.

Furthermore, from Table 1, where a comparison of the PSNR and the SSIM; and Figures 3 & 4 (g)-(l) where we present zoomed images of the ones in (a)-(f), we deduct that our approach leads to more significant and efficient results compare to the others. However, we notice a flat effect (see Figure 2 (f)), due to the PDEs inpainting approaches which is not able to perform texture reconstruction, while a texture synthesis step will be sometimes necessary.

In **Figure 5**, some of brain slices are presented to show the performance of our 3D-model in reproducing the fidelity of healthy parts, as shown in Figure 5 (c), (f) and (i). It should be noted that the artificial lesions of fixed volumes ($5 \times 5 \times 5$ voxel spheroids, see Figure 5 (b), (e) and (h)) are added to healthy brain and placed at multiple locations (infratentorial, periventricular and juxtacortical white matter locations) which is similar to lesions places seen in different patients with MS. According to the results in Figure 5 (c), (f) and (i), we can conclude that this model can give satisfactory results.
Note that the time variable in the PDE serves as an iteration parameter.

6. Conclusion

In this work, we proposed an image inpainting approach combining oriented diffusion based on the NLST, shock filtering and KMLS algorithm. We conclude that this approach is not only able to preserve the geometrical structures during the restoration process, but also eliminates the artifacts along the contours and in the vicinity/neighbourhood of structures. The contrast parameters estimation, adapted to the complexity of the structures contained in the image, has overcome the disadvantage of their adaptive choice. The experimental inpainting results, obtained in terms of SSIM, PSNR and visual quality, confirm the effectiveness of the proposed algorithm and is competitively compared to other algorithms (see Table 1 and Figures 1-5).

Furthermore we have to point out that:

1- The chosen stopping functions depending on the measure of the anisotropy provided by the NLST and the contrast parameters estimated at each iteration by

Algorithms 1 and 2 give a good compromise between robust orientation diffusion and shock filtering.

2- A smaller number of iterations can be used.

3- The incorporation of corner-and-edge-shock filters in (ZH) and (TV) methods can achieve better results.

4- Due to the estimation of the NLST and the contrast parameters at each iteration, more computation time is required.

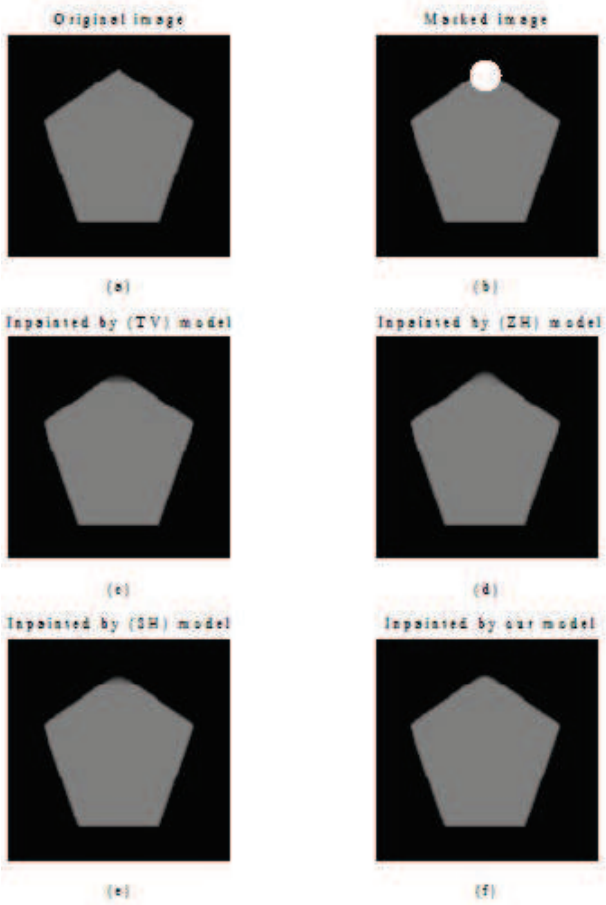

Figure 1: Inpainting results for a corner ($T = 290$).

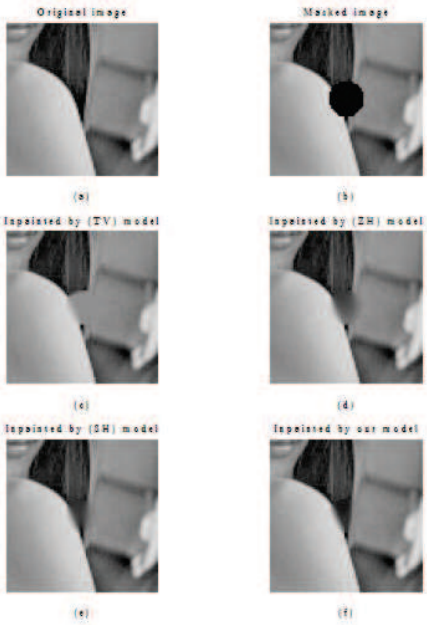

Figure 2: Inpainting results for a curvature ($T = 500$).

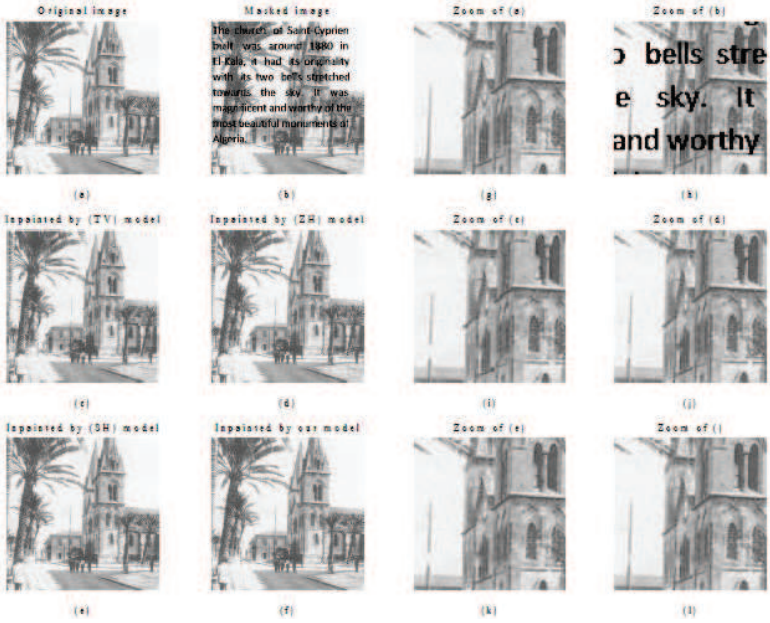

Figure 3: Text removal ($T = 400$).

Figure 4: Restoration of 50% of random missing pixels.

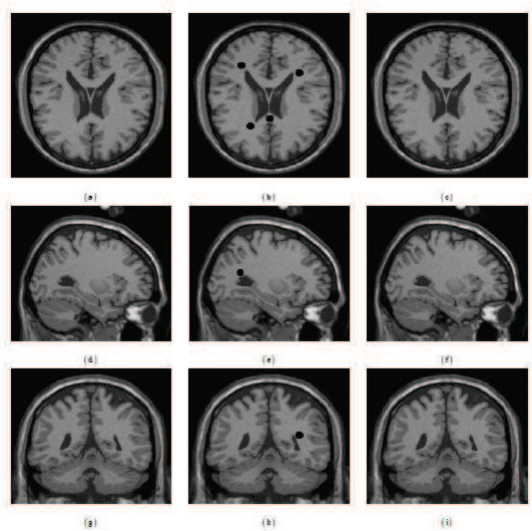

Figure 5: Inpainting of MS lesions in MRI image (a)-(d)-(g) : healthy brain slices for axial, sagittal and coronal section, (b)-(e)-(h) synthetic lesions simulation, (c)-(f)-(i), results of lesions filling

Acknowledgments

The authors are grateful to the referees for their valuable remarks and suggestions.

References

1. M. Battaglini, M. Jenkinson, and N. De Stefano, *Evaluating and reducing the impact of white matter lesions on brain volume measurements*, Hum. Brain Mapp., 33, pp.12062–2071, 2012.
2. M. Benseghir, F.-Z. Nouri, and P.-C. Tauber, *An Inpainting Result by a Nonlinear Structure Tensor*, Proceedings of the 20th International Conference on Information Visualisation (IV), pp.367– 370, 2016.
3. M. Bertalmio, G. Sapiro, V. Caselles, and C. Ballester, *Image inpainting*, Proceedings of the 27th Annual Conference on Computer Graphics and Interactive TechniquesComputer graphics, SIGGRAPH 2000, pp.417–424, 2000.
4. M. Bertalmio, L. Vese, G. Sapiro, and S. Osher, *Simultaneous structure and texture image inpainting*, IEEE transactions on image processing, 12(8), pp.882-889, 2003.
5. M. Bertalmio, *Strong-continuation, contrast-invariant inpainting with a third-order optimal PDE*, IEEE Transactions on Image Processing, 15(7), pp.1934-1938, 2006.
6. M. J. Black, G. Sapiro, D. H. Marimont, and D. Heeger, *Robust anisotropic diffusion*, in IEEE Transactions on Image Processing, vol. 7, no. 3, pp. 421-432, 1998.
7. M. Borroto-Fernández, M. González-Hidalgo, and A. León-Mecías, *New estimation method of the contrast parameter for the Perona-Malik diffusion equation*, Computer Methods In Biomechanics And Biomedical Engineering: Imaging and Visualization, Vol. 4 , No. 3-4, pp. 238-252, 2016.
8. T. Brox, J. Weickert, B. Burgeth, and P. Mrázek, *Nonlinear structure tensors*, Image and Vision Computing, Vol. 24, No. 1, pp.41–55, 2006.
9. T.-F. Chan and J. Shen, *"Mathematical models for local nontexture inpaintings"*, Journal of Applied Mathematics, Vol. 62 , No. 3, pp.1019–1043, 2001.
10. T.-F. Chan, and J. Shen, *Nontexture inpainting by curvature-driven diffusions*, Journal of Visual Communication and Image Representation 12(4), pp.436-449, 2001.
11. D.-T. Chard, J.-S. Jackson, D.-H. Miller, and C.-A-.M. Wheeler-kingscott, *Reducing the impact of white matter lesions on automated measures of brain gray and white matter volumes*, J. Magn. Reson. Imaging, 32, pp.223–228, 2010.
12. A. Criminisi, P. Perez, and K. Toyama, *Region filling and object removal by exemplar-based image inpainting*, in IEEE Transactions on Image Processing, vol. 13, no. 9, pp. 1200-1212, 2004.
13. I. Drori, D. Cohen-Or, and H. Yeshurun, *Fragment—based image completion*, ACM Transactions on Graphics, vol.22, pp. 303–312, 2003.
14. A.-A. Efros and T.-F. William, *Image quilting for texture synthesis and transfer* Proceedings of the 28th annual conference on Computer graphics and interactive techniques. ACM, pp.341-346, 2001.
15. M. Elad, J.-L. Starck, P. Querre, and D.-L. Donoho, *Simultaneous cartoon and texture image inpainting using morphological component analysis (MCA)*, Applied and Computational Harmonic Analysis, 19(3), 340-358, 2005.
16. C.W. Fang, and J.-J. Lien, *Fast image replacement using multi-resolution approach*, Computer Vision–ACCV, pp. 509-520, 2006.
17. C. Guillemot, M. Turkan, O. L. Meur, and M. Ebdelli, *Image inpainting using LLE-LDNR and linear subspace mappings*, in Proceedings of the IEEE International Conference on Acoustics, Speech , and Signal Processing (ICASSP '13), pp.1558–1562, 2013.

18. N. Guizard, K. Nakamura, P. Coupé, V.-S. Fonov, D.-L. Arnold, D.-L. Collins, *Non-Local Means Inpainting of MS Lesions in Longitudinal Image Processing*, Frontiers in Neuroscience, pp. 9:456, 2015.

19. M. Maouni, F.-Z. Nouri and D. Meskine, *Image Restoration by Non-standard Diffusion*, IEEE Geometric Modeling and Imaging , Modern Techniques and Applications, Vol. 9 , No. 11, pp.98–101, 2008.

20. S. Masnou,*Disocclusion : a variational approach using level lines*, IEEE Transactions on Image Processing, Vol. 11 , No. 2, pp.68–76, 2002.

21. P. Perona and J. Malik, *Scale-space and edge detection using anisotropic diffusion*, in IEEE Transactions on Pattern Analysis and Machine Intelligence, vol. 12, no. 7, pp. 629-639, 1990.

22. P. Peter, J. Weickert, A. Munk, T. Krivobokova, H. Li, *Justifying tensor-driven diffusion from structure-adaptive statistics of natural images*, In International Workshop on Energy Minimization Methods in Computer Vision and Pattern Recognition, Springer International Publishing, pp.263-277, 2015

23. A. Rares, M.-J. Reinders, and J. Biemond, *Edge-based image restoration*, IEEE Transactions on Image Processing, 14(10), pp.1454-1468, 2005.

24. M.-M.-O.-B.-B. Richard, and M.-Y.-S. Chang, *Fast digital image inpainting*, In Appeared in the Proceedings of the International Conference on Visualization, Imaging and Image Processing (VIIP), pp.106-107, 2001.

25. M. Sdika, and D. Pelletier, *Nonrigid registration of multiple sclerosis brain images using lesion inpainting for morphometry or lesion mapping*, Hum. Brain Mapp., 30: 1060–1067, 2009.

26. W. Shao and Z. Wei, *Edge-and-corner preserving regularization for image interpolation and reconstruction*, Image and Vision Computing, Vol. 26, No. 12, pp.1591–1606, 2008.

27. X. C. Tai, S. Osher and R. Holm, *Image Inpainting Using a TV-Stokes Equation*, Image Processing Based on Partial Differential Equations: Proceedings of the International Conference on PDE-Based Image Processing and Related Inverse Problems, pp.3–22, 2007.

28. D. Tschumperle and R. Deriche, *Vector-valued image regularization with PDEs: a common framework for different applications*, in IEEE Transactions on Pattern Analysis and Machine Intelligence, vol. 27, no. 4, pp. 506-517, 2005.

29. Z. Wang, A.-C. Bovik, H.-R. Sheikh, and E. P. Simoncelli, *Image quality assessment: From error visibility to structural similarity*, IEEE Transactios on Image Processing, vol. 13, no. 4, pp. 600-612, 2004.

30. J. Weickert, *Anisotropic diffusion*, in image processing vol. 1, pp. 59-60, 1998.

31. J. Wu, Z. Feng, and Z. Ren, *Improved structure-adaptive anisotropic filter based on a nonlinear structure tensor*, Cybernetics and Information Technologies, Vol. 14, No. 1, pp.112–127, 2014.

32. H. Yamauchi, J. Haber, and H.-P. Seidel, *Image restoration using multiresolution texture synthesis and image inpainting*, In Computer Graphics International, IEEE Proceedings, pp.120-125, 2003.

33. F. Zhang, Y. Chen, Z. Xiao, L. Geng, J. Wu, T. Feng, P. Liu, Y. Tan, and J. Wang, *Partial Differential Equation Inpainting Method Based on Image Characteristics*, Image and Graphics: 8th International Conference, pp.11–19, 2015

M. Benseghir,
F.Z. Nouri,
Mathematical Modeling and Numerical Simulation Laboratory
Faculty of Sciences, Badji Mokhtar University,
BP 12 Annaba 23000, Algeria.
E-mail address: bens.moun.ma@hotmail.fr
E-mail address: fz_nouri@yahoo.fr, (Corresponding author)

and

P.C. Tauber,
Faculty of Medicine,
INSERM U930 Eq.3, bureau J4-430
10 bd Tonnelle Tours 37032, France.
E-mail address: clovis.tauber@univ-tours.fr